

**ANALYSIS OF HIGH SPEED RADially ROTATING HIGH-
TEMPERATURE HEAT PIPES**

By

LUIS O. GONZALEZ

**A thesis submitted in partial fulfillment of the requirements
for the Honors in the Major Program in Mechanical Engineering
in the College of Engineering and Computer Science
and in the Burnett Honors College
at the University of Central Florida
Orlando, Florida**

Fall Term 2007

Thesis Chair: Dr. Ali P. Gordon

Abstract

Internal convective cooling is a method by which components, such as gas turbine blades, are protected from damage caused by elevated temperatures. Heat pipes are structures that transport and dissipate large quantities of pressurized thermal energy. The thermal energy is transported from a heat source to a thermal sink via evaporative cooling. A radially rotating high temperature heat pipe employs centrifugal force to return or drive the working saturated-vapor mixture from the condenser section to the evaporator section. A rotating heat rig is being developed at the University of Central Florida (UCF) in order to gain a better understanding of the interaction between thermal conductivity, rotational speed, operating temperatures and thermal loads. As a part of its development, this study will focus on identifying key factors that maximize the first critical speeds on rotating heat pipe assemblies having non-uniform temperature distributions. It was found that in order to avoid reaching the first critical speed the use of double bearings should be implemented. Since the temperature of the heat pipe will be non-uniform, this will have a minimal effect on the critical speed of the rotating rig. The first phase of the construction of the rotating rig will be stable and will provide valuable test data without reaching any critical speeds.

Acknowledgements

I would like to thank Dr. Ali P. Gordon for all the advice and guidance through this project and throughout my undergrad education. I would also like to thank the NASA Glenn Research Center under SUS of Florida Turbine Initiative for funding this research project. Outstanding members of this research project were Steve and Robby who helped me during this project but who will also take this research to the next phase. Lastly, I would like to thank the University of Central Florida for preparing me to be successful in my career but also in life.

Table of Content

1. Introduction.....	1
2. Literature Review.....	6
3. XLRotor Rotordynamic Analysis	17
3.1. Undamped Critical Speeds.....	17
3.2. Undamped Critical Speed Mode Shapes.....	18
4. Results.....	19
4.1 Assumptions.....	20
4.2. Single Bearings	21
4.3. Double Bearings.....	25
4.4. Non-uniform Temperature Distribution.....	28
4.5. Turbine Blades	31
5. Discussion and Conclusion	34
6. Future Development.....	35
7. Appendix: List of Symbols/Abbreviations	36
8. References.....	37

List of Figures

Figure 1: Diagram of turbine blade with internal cooling channels.	2
Figure 2: Conceptual design of UCF rotating heat pipe rig.....	3
Figure 3: FIU schematic of the testing apparatus (Ling, 2001).	10
Figure 4: Closed-form analytical solution versus experimental data of temperature distribution (Ling, 2001).....	12
Figure 5: Temperature distribution at the start-up process (Ling, 2001).....	14
Figure 6: Heat inputs versus temperature distribution across the heat pipe (Ling, 2001). 15	
Figure 7: Temperature distribution with different rotating frequencies (Ling, 2001).	16
Figure 8: Single bearing supported shaft using XLRotor.	22
Figure 9: Undamped critical speed map for single support bearings.....	23
Figure 10: Undamped critical speed 1st, 2nd and 3rd mode shape plots using single support bearings.....	24
Figure 11: Double bearing supported shaft using XLRotor.....	25
Figure 12: Undamped critical speed map for double support bearings.	26
Figure 13: Undamped critical speed 1st, 2nd and 3rd mode shape plots using double support bearings.....	27
Figure 14: Double bearing supported and non-uniform temperature distribution shaft using XLRotor.	28
Figure 15: Undamped critical speed map for double support bearings and non-uniform temperature distribution.....	29
Figure 16: Undamped critical speed 1st, 2nd and 3rd mode shape plots using double support bearings and non-uniform temperature distribution.	30

Figure 17: XLRotor model of a shaft using double support bearings and turbine blades simulated as a weight at the center.	31
Figure 18: Undamped critical speed map for double support bearings and turbine blades.	32
Figure 19: Undamped critical speed 1st, 2nd and 3rd mode shape plots using double support bearings and turbine blades.....	33

1. Introduction

Traditionally, industrial gas turbine (IGT) blades have been cooled internally through a series of internal channels. The channels carry a working fluid that circulates while it dissipates excess thermal energy, protecting the blades from damage caused by elevated temperatures, as shown in Fig.1. Finding new and innovative methods of cooling these blades has sparked research on other efficient ways of dissipating heat, such as heat pipes. Heat pipes are known to have a high thermal conductance and the ability to transfer large amounts of heat with a relatively simple passive structure. The thermal energy that is absorbed in the evaporator section from a heat source is allowed to cool in the condenser section where the thermal energy is dissipated to a thermal sink. Their ability to transport thermal energy has made them extremely useful in modern computer applications and an increasingly important role in managing spacecraft internal temperatures by drawing excess heat from temperature sensitive components. The working fluid inside the heat pipe is chosen so that the fluid is a saturated-vapor mixture at its operating temperature (Razani et al., 2006). Heat pipes are also resistant to high temperature environments, such as simulated turbine blade conditions. Experimental data prove that radially rotating high temperature heat pipes have a high and effective thermal conductance. The thermal conductance has been established to be 60 to 100 times higher than the thermal conductance of copper (Ling et al., 2001). Combining heat pipes with traditional turbine blade cooling represents a new cooling method (Ling et al., 2001). Several rotating heat pipe rigs have been used to conduct a variety of Fluid Structure Interactions (FSI) experiments. The device that serves as a benchmark for the University

of Central Florida (UCF) design was fabricated at Florida International University (FIU).

A schematic of the testing apparatus that is being constructed at UCF is shown in Fig. 2.

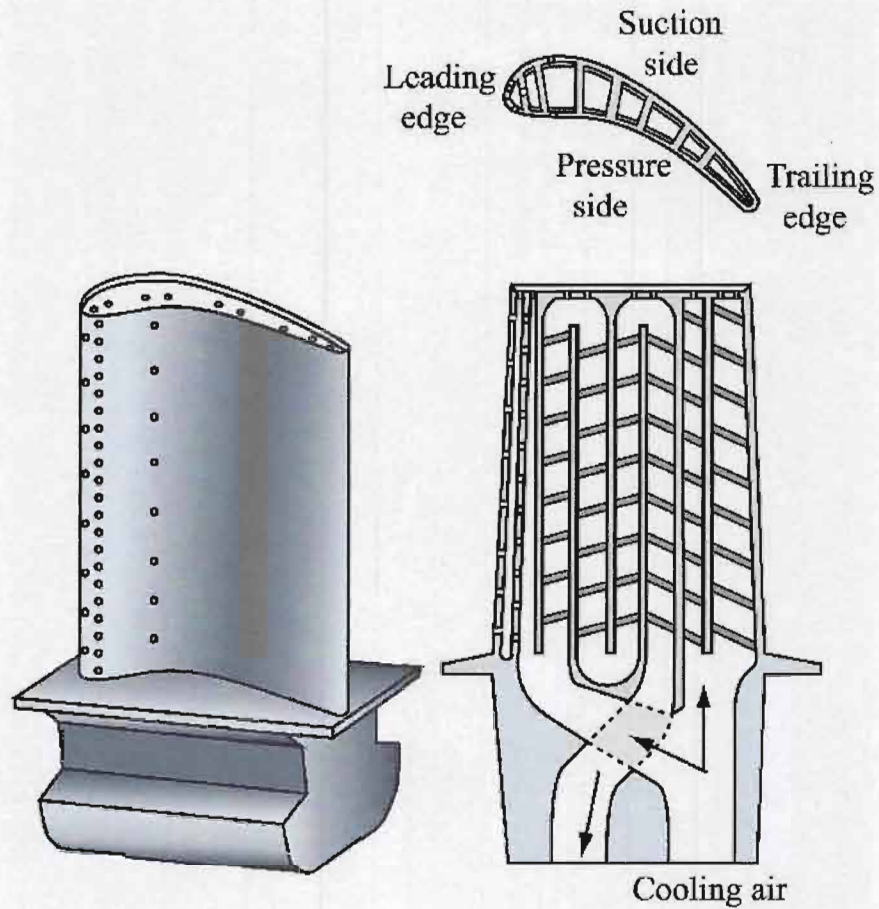


Figure 1: Diagram of turbine blade with internal cooling channels.

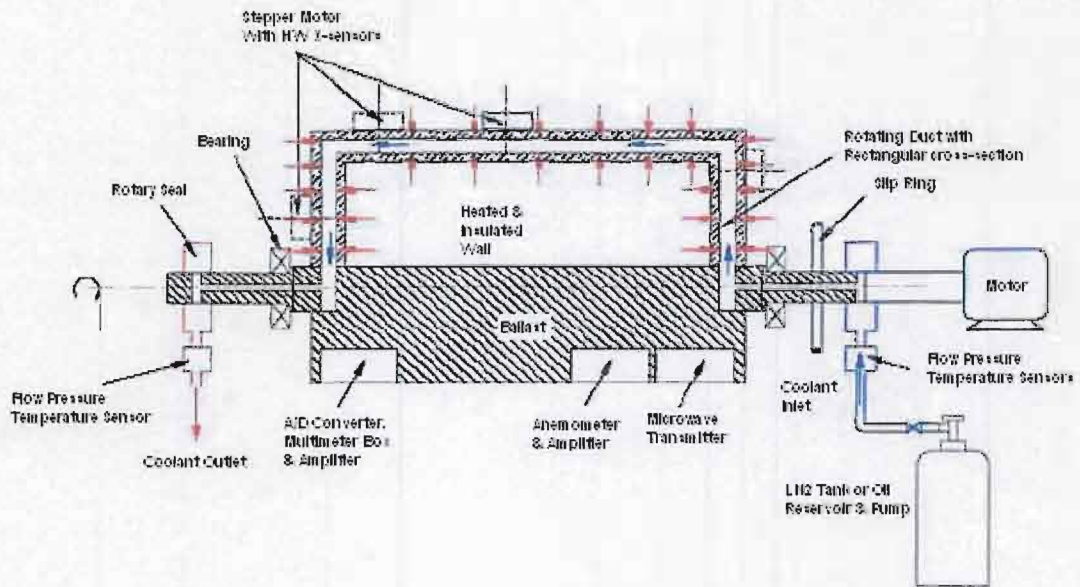


Figure 2: Conceptual design of UCF rotating heat pipe rig.

The ability to spin test components allows valuable test data earlier in the design process, which helps reduce costly engineering redesigns and lowers the risk of in-service component failure. Additional research on testing methods, therefore, is continuing. Historically, experimental investigations of mechanical durability have typically been carried out on two distinct size scales: (1) full scale component testing under realistic service conditions and (2) specimen size testing under highly idealized conditions. While each of these techniques has their advantages and disadvantages, more attention is being garnered by intermediate scale experiments. In these situations, components from turbine systems are reduced to a smaller scale without appreciable change in geometry. The service conditions to which they are subjected are slightly idealized. Structural, thermal, fluidic, and FSI experiments more closely resemble service conditions. One such intermediate scale testing device is that of the radially rotating heat pipe. The rotating

test rig being designed and fabricated at UCF, is an on-going research effort focused on subjecting scaled down components to mildly idealized service conditions. In this manner of intermediate durability testing, attributes of the structural and fluid-structure interaction (FSI) capabilities of the rotating heat pipe will be characterized. The results and conclusions derived from the intermediate scale-testing will serve valuable for future full-scale experiments performed.

Although the FIU rig has been extremely useful for heat transfer experiments (e.g. temperature distribution, absorption of heat and thermal conductance across the heat pipe), a system capable of more closely simulating realistic service conditions is needed. The apparatus built at UCF was designed to operate at angular velocities of 10,000 RPM. This speed is an improvement to other testing apparatus and is closer to highly advanced land-based industrial gas turbines (IGT). By spin testing at higher angular speeds, heat transfer experiments can be modeled more accurately. The research performed will focus more on mechanical interactions experienced within the heat pipe. As a part of this research this study will focus on identifying key factors that maximize the first critical speeds on rotating heat pipe assemblies having non-uniform temperature distributions. From these new experiments a better understanding of the interaction between thermal conductivity, rotational speed, operating temperatures and heat loads can be observed.

To support the development of the UCF rotating heat rig device, aspects of the rotating rig assembly will be analyzed for temperature effects and critical speeds. This study will also focus on shaft optimization in order to reach a desired maximum operational speed of 30,000 RPM. A large portion of the research will focus on performing the adequate calculations that analyze the shaft and testing specimen. The

analytical study will focus on a straight shaft testing specimen held in place by contact ball bearings. Another large portion of the analysis will concentrate on the critical speed analysis of the shaft and the different mode shapes. The software package XLRotor, will be used to perform the rotordynamic analysis. It allows parametric designing using different rotating speeds, temperature distributions and bearing locations without building. XLRotor also takes into account the fluctuating torque and fluctuating moment that is experienced in combination. Since the rotating components will be experiencing temperatures nearing gas turbine conditions, selecting the proper material and its dimensions that could sustain the stresses associated with high rotational speeds is crucial.

Understanding the limitations of the system is crucial; as such, a thorough analysis will be performed obtaining relevant data that will aid in the design process. The correlation of critical speeds as at a specific temperature will be explored in order to derive an analytical model that accounts for the temperature increase from start-up to its operational temperature. Since the results will be derived from intermediate scale testing, which idealizes turbine conditions, the proper conclusions must be drawn in order to proceed with full scale testing in the future.

2. Literature Review

A heat pipe is a heat transfer mechanism that can transport large amounts of heat between the heat pipe and a source. Heat pipes employ evaporative cooling to transfer thermal energy from one point to another by the evaporation and condensation of a working fluid or coolant. Most research efforts have been focused on radially rotating high temperature heat pipes. A radially rotating, high temperature, heat pipe employs centrifugal force to return or drive the working condensate fluid to the evaporator section, in order to transfer heat from a heat source and a heat sink. Heat pipes are known to be passive devices and have simple structures, high thermal conductance and the ability to transfer large amounts of heat. The working fluid inside the heat pipe is chosen so that at the desired operating temperature, the fluid is a saturated-vapor mixture (Razani et al., 2006). Heat pipes are also resistant to high temperature environments, such as simulating turbine blade conditions. Combining heat pipes with traditional turbine blade cooling represents a new cooling method (Ling et al., 2001). In order for the heat pipe to perform as expected, the heat pipe needs to be designed to ensure that the working fluid circulates properly during all operational phases (Razani et al., 2006). Typically, the performance of a rotating heat pipe is evaluated by determining how the overall thermal conductivity is affected by changes in rotational speed, operating temperatures and heat loads. In the radially rotating heat pipe, the longitudinal axis of the heat pipe is perpendicular to the axis of rotation, with the evaporator section furthest away from the axis of rotation. This is critical in order to use the centrifugal force to return the fluid back to the condenser section.

Several rotating heat pipe rigs have been used to conduct a variety of fluid-structure interaction (FSI) experiments. The device that was designed and fabricated at institutions such as FIU has been used mainly for heat transfer experiments. These heat transfer experiments include the analysis of the temperature distribution, absorption of heat and thermal conductance across the heat pipe.

The temperature distribution along the heat pipe length, without an adiabatic section, can be expressed by the following relations. The nomenclature for these equations can be found in the Appendix. The evaporator section can be modeled by the following equation:

$$T_{v,z} = T_{v,e} - \frac{T_v F_v Q_c}{h_{fg} \rho_v \sin(\phi)} \left\{ L_{eff} - \left[L - \frac{(L^2 - Z^2)}{L - L_c} \right] \right\} - \frac{T_v \omega^2 \sin(\phi)}{h_{fg}} \left[\left(Z_0 + \frac{1}{2} Z \right) Z \right] ; L_c \leq z \leq L \quad (1)$$

The condenser section can be modeled by the following equation:

$$T_{v,z} = T_s + a - \Delta T_{v,L} + \Delta T_{v,z} + a[e^{(mZ)^{-1}}] ; 0 \leq z \leq L_c \quad (2)$$

The condenser section can also be modeled by the following equation:

$$T_{v,z} = \Delta T_{v,L} - \Delta T_{v,L} + \Delta T_{v,L_c} - c[e^{(m(2L_c - Z))} - e^{(mZ)}] ; L_c \leq z \leq L_c \quad (3)$$

Where,

$$m = \left[\frac{2r_o h_c}{k_p [(r_o)^2 - (r_i)^2]} \right]^{\frac{1}{2}} \quad (4)$$

Neglecting the diffuse effects of non-condensable gases is given by the following equation:

$$\Delta T_{v,z} = \frac{T_v F_v Q_c}{2h_{fg} \rho_v \sin(\phi)} Z^2 + \frac{T_v}{h_{fg}} [\omega^2 (Z_o + \frac{1}{2} Z \sin(\phi)) Z] ; 0 \leq Z \leq L_c \quad (5)$$

$$\Delta T_{v,z} = \frac{T_v F_c Q_c}{2h_{fg} \rho_v \sin(\phi)} \left[L - \frac{(L-Z)^2}{L-L_z} \right] + \frac{T_v}{h_{fg}} [\omega^2 (Z_o + \frac{1}{2} Z \sin(\phi)) Z] ; L_c \leq Z \leq L \quad (6)$$

Based on the analytical solutions, it follows that the temperature distribution along the heat pipe is a function of the rotating speed, the size of the heat pipe, fluid properties, heat inputs in the evaporator sections, cooling conditions in the condenser section and the effects of the non-condensable gases.

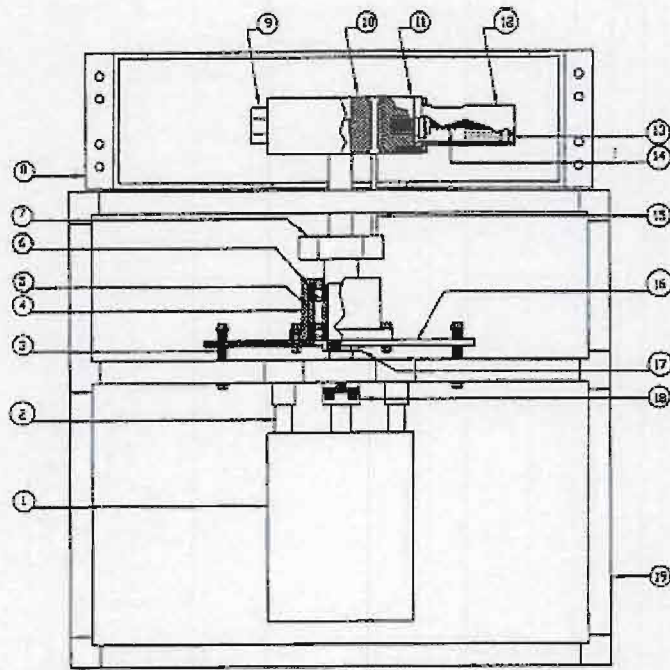
In order to prevent damage to the apparatus or operators, it is imperative that the critical speeds of the rotating rig are calculated. Failure to calculate the critical speeds will result in the heat pipe going into resonance and damaging other components. The first critical speed is determined by the bending characteristics of the rotor (Streby et al., 1996). The equation for the first critical speed is given as:

$$N = 30 \frac{\omega}{\pi} \quad (7)$$

The critical speeds at other support stiffnesses can be calculated by the following equation (Streby et al., 1996):

$$[(2K - \omega^2 \rho AL) \left(\frac{EI\pi^4}{2L^3} - \omega^2 \rho A \frac{L}{2} \right) - \omega^4 (4\rho^2 A^2 \frac{L^2}{\pi^2})] = 0 \quad (8)$$

A high-speed rotating apparatus was constructed at FIU to test the effectiveness of radially rotating high temperature heat pipes. The FIU set up was successful in achieving experimental data. A schematic of the testing apparatus is shown in Fig. 3.



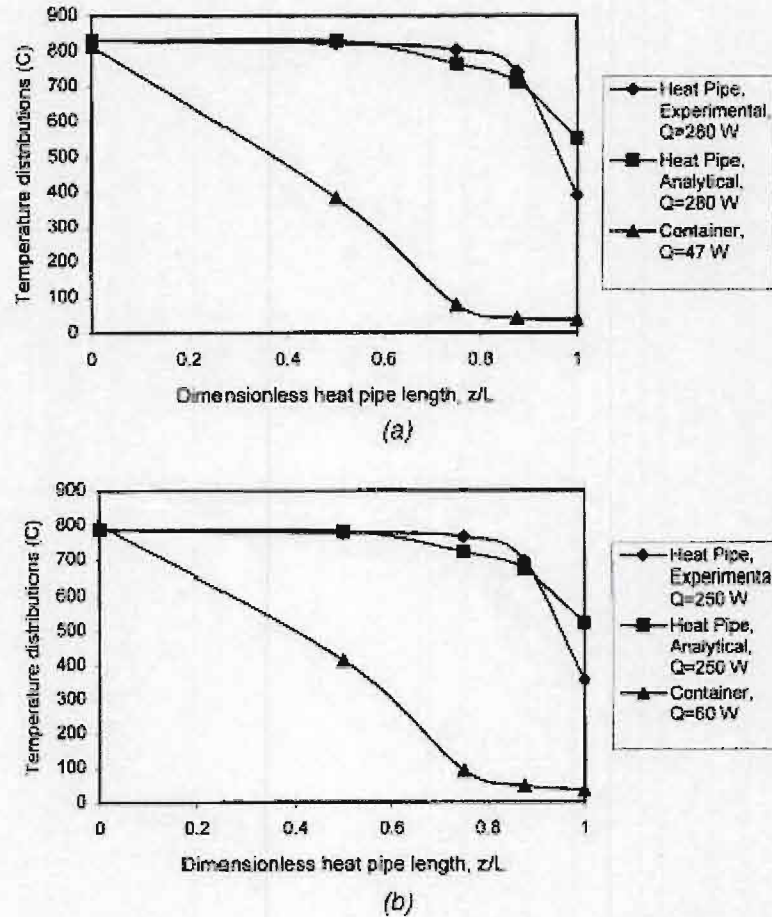
1	Motor	8	Protective Shell	15	Thermocouples
2	ConnectingBar	9	Balancing Weight	16	Bearing Platform
3	Springs	10	Inner Cylinder	17	Bearing Nut
4	Bearing House	11	Outer Cylinder	18	Flexible Coupling
5	Spacer	12	Heater Cap	19	Frame
6	Bearing House	13	Heater		
7	Slip Rings	14	Heat Pipe		

Figure 3: FIU schematic of the testing apparatus (Ling, 2001).

The variable parameters that could be adjusted are as follows: (1) the angular velocity of the test apparatus (2) the heat input to the evaporator section and (3) the flow rate of the cooling fluid in the condenser section. One of the major issues of the apparatus is controlling the vibrations caused by the rotational effects. In the FIU setup, a motor drives the shaft with a revolution range up to 3600 RPM. In order to control the vibration caused by the shaft rotor, a flexible coupling was used to connect the shaft with the rotor. The springs connecting the rotor to the frame act as a dampening system for small vibrations due to a slight unbalance. There are two slip rings mounted on the shaft. These

rings are used to supply the electrical current from the power transformer and the temperature measuring equipment. The type of thermocouple used depends on the specific application and will need to be determined by the operating temperatures experienced inside the testing apparatus. A proper method has to be implemented to properly balance the rotor system inside the testing section, for the specific application. FIU implemented the use of a counter weight in order to balance the system. Another balancing method is to use dynamic balancing of the components (Streby et al., 1996). Each component is balanced using a computer balancing system. Each time components are changed they will have to be dynamically balanced, which could prove costly. It has also been found that incorporating magnetic shaft seals and several types of cooling sprays caused the vibration behavior of the system to be drastically different and its effects should be investigated (Streby et al., 1996). The following experiments were based on the geometry, as shown in Fig. 3.

Experimental data prove that radially rotating high temperature heat pipes have a high and effective thermal conductance. The thermal conductance has been established to be 60 to 100 times higher than the thermal conductance of copper (Ling et al., 2001). To illustrate the effectiveness of the heat pipes a comparison of the closed-form analytical solution and experimental data is shown in Fig. 4.



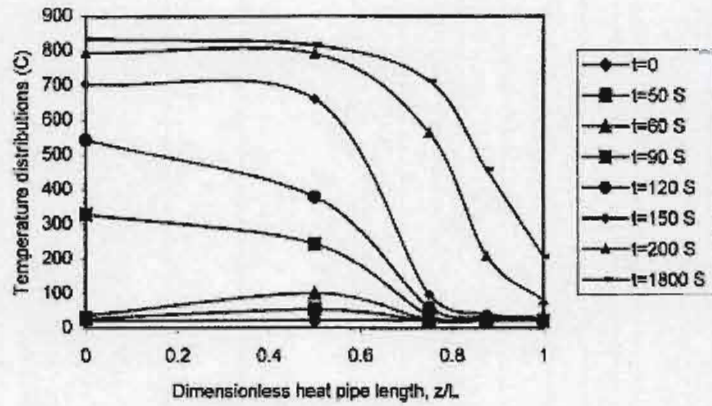
Comparisons of temperature distributions and heat inputs between the experimental data, closed-form analytical solution ($L_{c,n}=4$ mm), and the heat pipe container: (a) $\omega^2 \bar{Z}_a / g = 470$, $d_i = 2$ mm, $W = 6.7 \times 10^{-3}$ m³/s; (b) $\omega^2 \bar{Z}_a / g = 470$, $d_i = 1.5$ mm, $W = 6.7 \times 10^{-3}$ m³/s.

Figure 4: Closed-form analytical solution versus experimental data of temperature distribution (Ling, 2001).

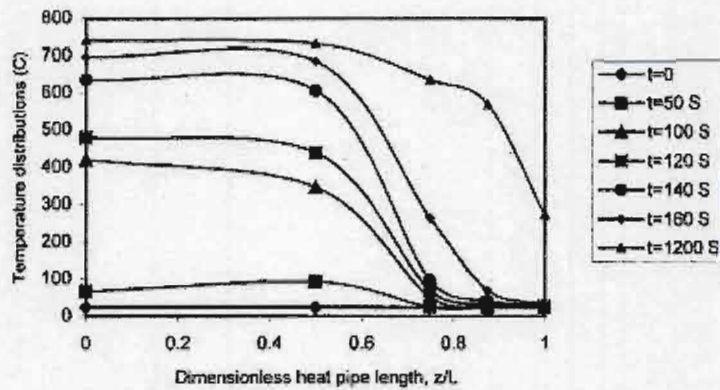
Clearly, there is strong agreement between the analytical solution and the experimental data. These comparisons prove that radial rotating high temperature heat pipes are effective in transferring heat across the pipe. They have much higher heat transfer capabilities than any metal available. It can also be seen that the temperature distribution across the heat pipe is nearly uniform in the evaporator section; however

there is a temperature gradient that exists in the condenser section, which is most likely attributed to the non-condensable gases. It is unavoidable that a small amount of non-condensable gases is trapped in the heat pipe during the charging process and sealing. In some cases charging the condenser end with non-condensable gases will prevent the end, which may be attached to heat sensitive components, from becoming too hot (Ling et al., 2000). Due to the way the condenser section is located on the apparatus, an unavoidable heat sink is created. The temperature distribution in this section is lower than the rest of the heat pipe length, which causes a deviation from the analytical solution. The analytical solution accounts for the effect of the non-condensable gases but does not account for the effects of the heat sink that is formed.

The start up behavior of the heat pipe can be seen as the heat pipe begins to work. The retardation of the heat pipe temperature to increase is due to the fact that the working fluid inside the evaporator section was not yet vaporized. Once the temperature increased inside the heat pipe, the heat pipe began to work properly. It took approximately 1200s for the heat pipe to become operational (Ling et al., 2001). The temperature distribution at startup is shown in Fig. 5.



(a)



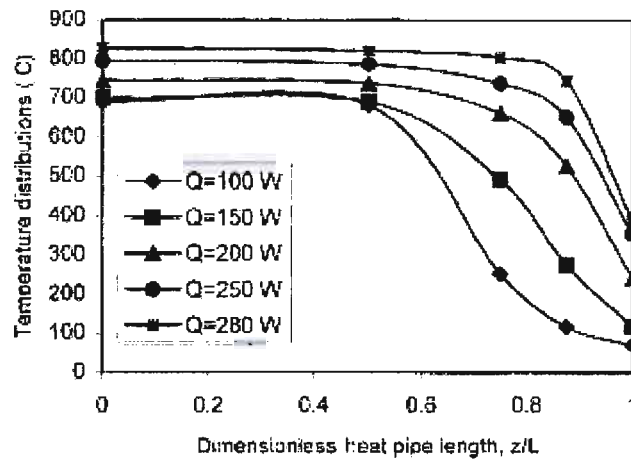
(b)

Temperature distributions along the heat pipe length with the diffuse effects of non-condensable gases during the heat pipe startup process: (a) $\omega^2 \bar{Z}_3 / g = 470$, $d_f = 1.5$ mm, $Q = 176$ W; (b) $\omega^2 \bar{Z}_3 / g = 470$, $d_f = 2$ mm, $Q = 175$ W.

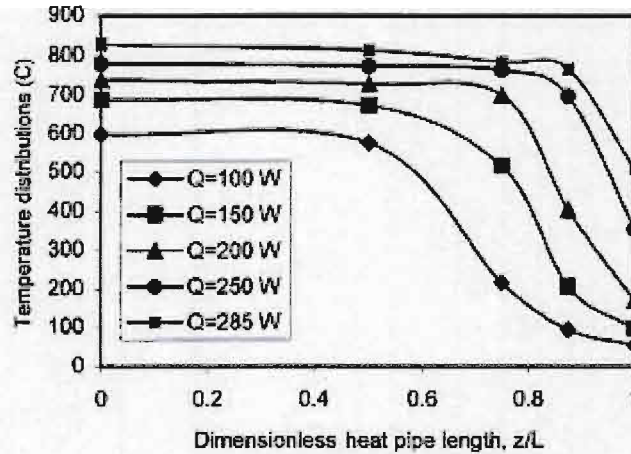
Figure 5: Temperature distribution at the start-up process (Ling, 2001).

The effects of heat input is one of the major parameters that need to be examined. At low heat inputs in the evaporator section, the condenser section will remain inactive with its temperature remaining close to the cooling fluid temperature. Once the heat inputs are increased, the temperature rises across the heat pipe into the condenser area where the heat pipe begins to be functional. With a low heat input and a high rotating speed, a higher heat transfer coefficient occurs, so only a small part of the condenser

section will remain functional. The heat transfer characteristics and effective heat conductance of the heat pipe will improve significantly once the heat inputs are increased. Fig. 6 shows the effects of heat inputs versus the temperature distribution across the heat pipe.



(a)

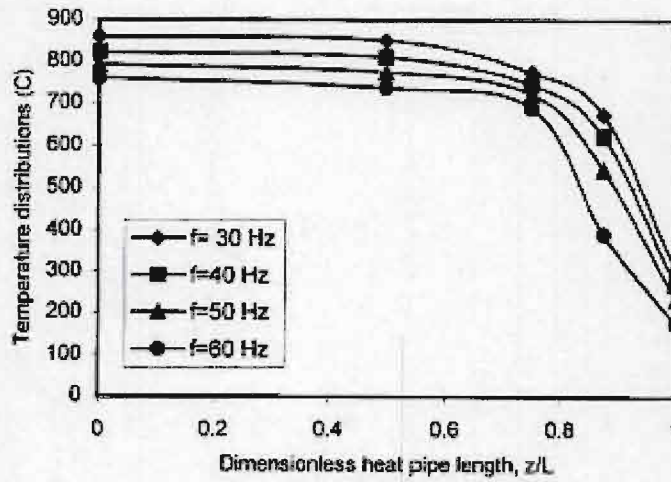


(b)

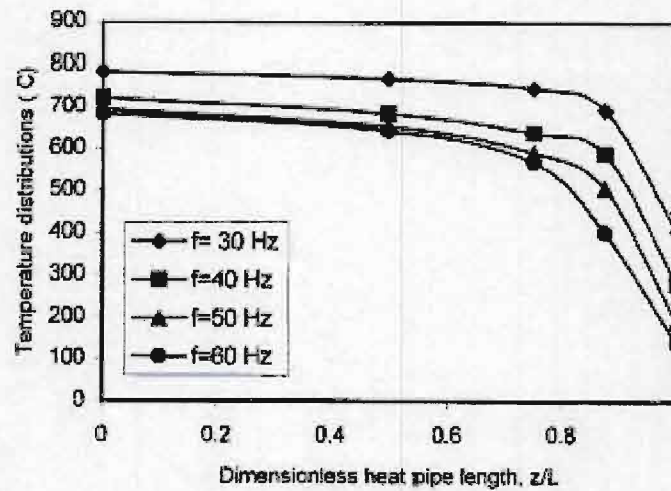
Temperature distributions along the dimensionless heat pipe length with different heat inputs: (a) $\omega^2 Z_s / g = 470$, $d_i = 2$ mm, $W = 6.7 \times 10^{-3}$ m²/s; (b) $\omega^2 Z_s / g = 470$, $d_i = 1.5$ mm, $W = 6.7 \times 10^{-8}$ m²/s.

Figure 6: Heat inputs versus temperature distribution across the heat pipe (Ling, 2001).

With an increase of the dimensional centrifugal forces, the vapor pressure and temperature drop will be increased across the heat pipe length. Fig. 7 shows the effects of different rotating frequencies versus temperature distribution across the heat pipe length.



(a)



(b)

Temperature distributions along the dimensionless heat pipe length with different rotating frequencies: (a) $Q = 225$ W, $d_i = 1.5$ mm; (b) $Q = 225$ W, $d_i = 2$ mm.

Figure 7: Temperature distribution with different rotating frequencies (Ling, 2001).

3. XLRotor Rotordynamic Analysis

In order to construct a rotating rig that closely characterizes turbine blade conditions extensive rotordynamic analysis was performed. Turbine blade conditions exceed 10,000 RPM and temperatures in excess of 500° Celsius. When designing a high speed, high temperature rotating apparatus, a minimal unwanted vibration could cause damage to the system or the operators. XLRotor 3.0 is a rotordynamic analysis program that is used to design and maintain rotating equipment in industry since 1995. It uses the Finite Element Method where specially optimized sparse matrix algorithms are employed. XLRotor is compatible with any versions of Excel and Windows operating systems. The results are tabulated in spreadsheet format and can perform a multitude of calculations and plots. This program is compatible with other programs; all that is required is to create an Excel spreadsheet driver for your program using the template that comes with XLRotor. Using XLRotor, the undamped critical speeds (UCS), undamped critical mode shapes and the damped eigenvalue natural frequency will be analyzed for a straight shaft. The trial version of XLRotor was used and is limited to five stations.

3.1. Undamped Critical Speeds

The critical speed is the theoretical angular velocity in which a shaft goes into resonance, due to the residual unbalance after balancing the shaft. When a shaft reaches its critical speed, the shaft begins to excessively vibrate. This excess vibration would ultimately cause a catastrophic failure of the system that could both damage the system or injure the operator. The critical speed of a shaft is a function of the unbalance force and the rotational speed. XLRotor analyzes the UCS by reducing all the bearings to simple undamped axis-symmetrical springs such that $K_{xx}=K_{yy}$ and $K_{xy}=K_{yx}=0$. This means that the bearing supports allow the shaft to rotate freely without a dampening effect. The rotor transverse inertia is replaced with the transverse minus the polar inertia (I_t-I_p). This modification constrains the rotor rotational speed because of gyroscopic. The UCS command in XLRotor computes such eigenvalues directly, without the need to iterate the rotor speed. It also provides the 2nd, 3rd and 4th critical speed maps for a range of support stiffness value.

3.2. Undamped Critical Speed Mode Shapes

When designing shafts, it is important to study the mode of rotation or oscillation due to unwanted vibrations. When the shaft vibrates, it oscillates according to some specific fundamental oscillation; however, a typical system has an infinite number of modes. They include the basic modes, which correspond to the first three fundamental modes. The fundamental modes are generally the most important, because they stress the structure the most. They are the two flexional modes (along two directions, orthogonal to each other) and the third torsional mode. XLRotor calculates the mode shapes for the oscillation experienced. The bearing supports are modeled as undamped axis-symmetrical springs, which allow the shaft to rotate freely. It is critical to analyze the mode shapes, since this allows for a safe design.

4. Results

In order to justify how the heat pipe rotating rig was designed it was crucial to test different configurations that would maximize the first critical speed. The limitation of the motor that would supply the rotational power would only produce approximately an angular velocity of 10,000 RPM. Testing different bearing configurations and the length of the testing section would justify a solution such that the first critical speed of the system would not impact the heat pipe. The different support configurations that were tested were single and double bearings. The heat pipe will also be subjected to non-uniform temperature distribution by heating at certain sections along its testing length. Since, the ultimate goal of this research is to aid the design of a rotating apparatus that supports turbine blades; a straight shaft with the weight of the blades located at the center was analyzed. For all these configurations, a critical speed map and the first three mode shape plots were created.

4.1 Assumptions

In order to begin collecting and analyzing data, the assumptions of the research must be clearly stated. This is an important step since the data collected is dependent on the conditions that are assumed. The Table 1 is the list of assumptions that were used as part of the research.

Table 1: List of assumptions.

No.	Assumption	Application
1	10,000 lb/in. Bearing Stiffness	Critical speed map plots as a function of bearing stiffness. <i>Note:</i> Bearing stiffness can be considered a displacement-force relation.
2	Carbon Steel Shaft	Shaft will be constructed out of carbon steel.
3	Modulus of Elasticity equal to 30×10^6 psi	This Modulus of Elasticity is at room temperature and will be used when uniform temperature is specified.
4	Modulus of Elasticity equal to 26×10^6 psi	This Modulus of Elasticity is 500° Celsius and will be used when non-uniform temperature distribution is specified.
5	Turbine Blades Modeled as weight located at the center of the shaft	Used to model turbine blades

4.2. Single Bearings

XLRotor was used to model single bearing supports located at the end of the shaft, as shown in Fig. 8.

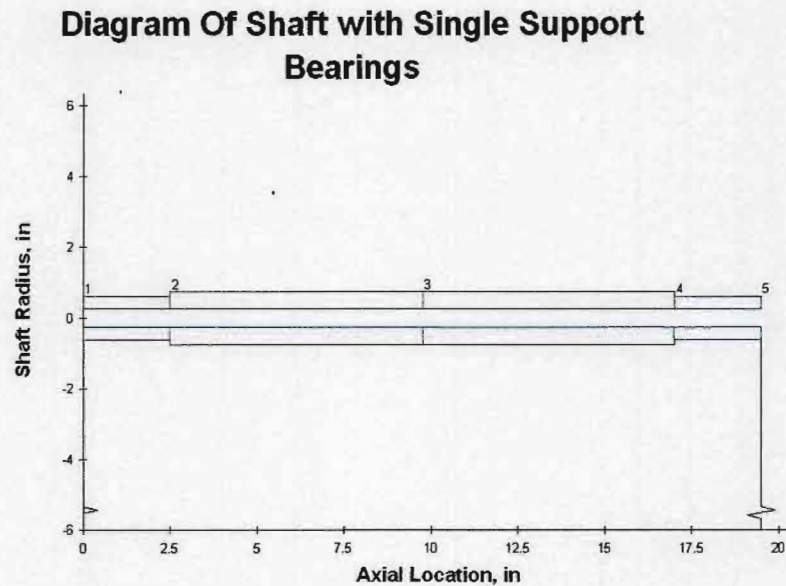


Figure 8: Single bearing supported shaft using XLRotor.

The shaft that was modeled contains two 1.25 inch diameter shaft of 2.5 inch length located at the ends of the shaft. This section is where the single bearings will be located. They are represented by the spring symbol located at the ends of the shaft. The model also contains a 1.50 inch diameter and 15 inch long stepped shaft. The inner diameter of the entire shaft is maintained at 0.5 inch throughout.

Using single bearings at the end of the heat pipe rotating rig the following undamped critical speed map was created, as shown in Fig. 9. The first, second and third critical speed maps are represented by cpm1, cpm2 and cpm3, respectively.

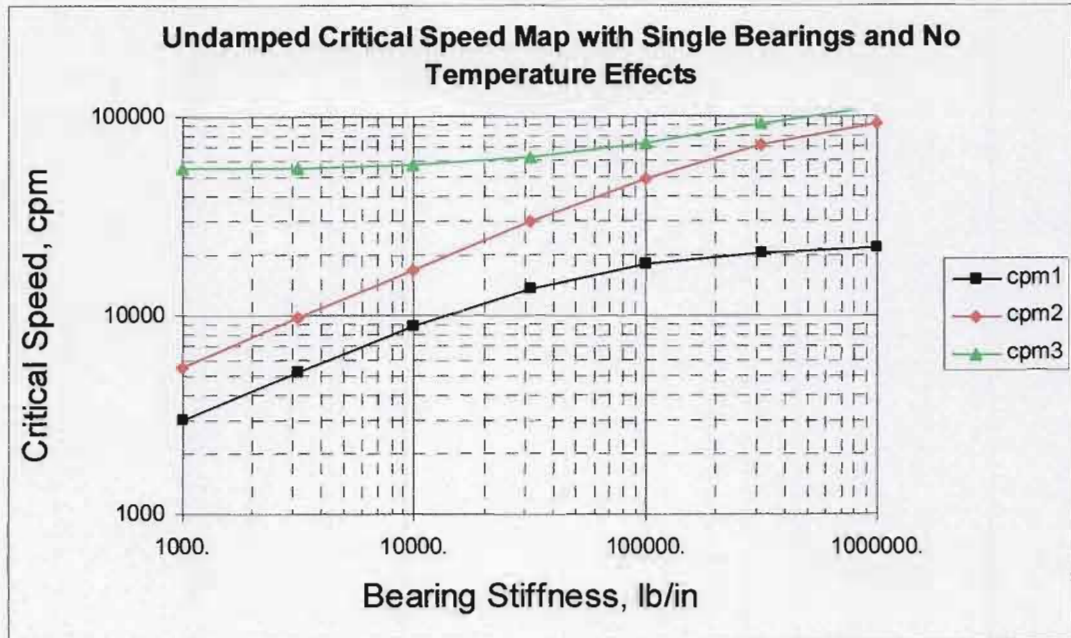


Figure 9: Undamped critical speed map for single support bearings.

XLRotor created the critical speed map (cpm) as a function of bearing stiffness. A bearing stiffness of 10,000 lb/in is assumed at the ends of the shaft. Table 2 shows the critical speeds at different support stiffnesses, where the bold specifies the relevant critical speeds to the research.

Table 2: Undamped critical speed table for single support bearings at different support stiffness values.

Stiffness	cpm1	cpm2	cpm3
1000.	2960.8	5532.9	54594.6
3162.	5176.6	9803.2	55198.0
10000.	8751.4	17241.9	57037.7
31623.	13582.4	29691.3	62218.2
100000.	18100.4	48578.3	74031.6
316229.	20710.6	71984.8	92442.9
1000000.	21766.0	92432.1	110005.9

Fig. 10 shows the mode shape plots using single support bearings located at the end of the rotating rig. The first two mode shapes are considered the rigid body modes of the system. When the system reaches these two critical speeds the shaft begins to oscillate in the fundamental form specified. The third mode shape is often called the bending mode. This is considered the most important since it stresses the system the most.

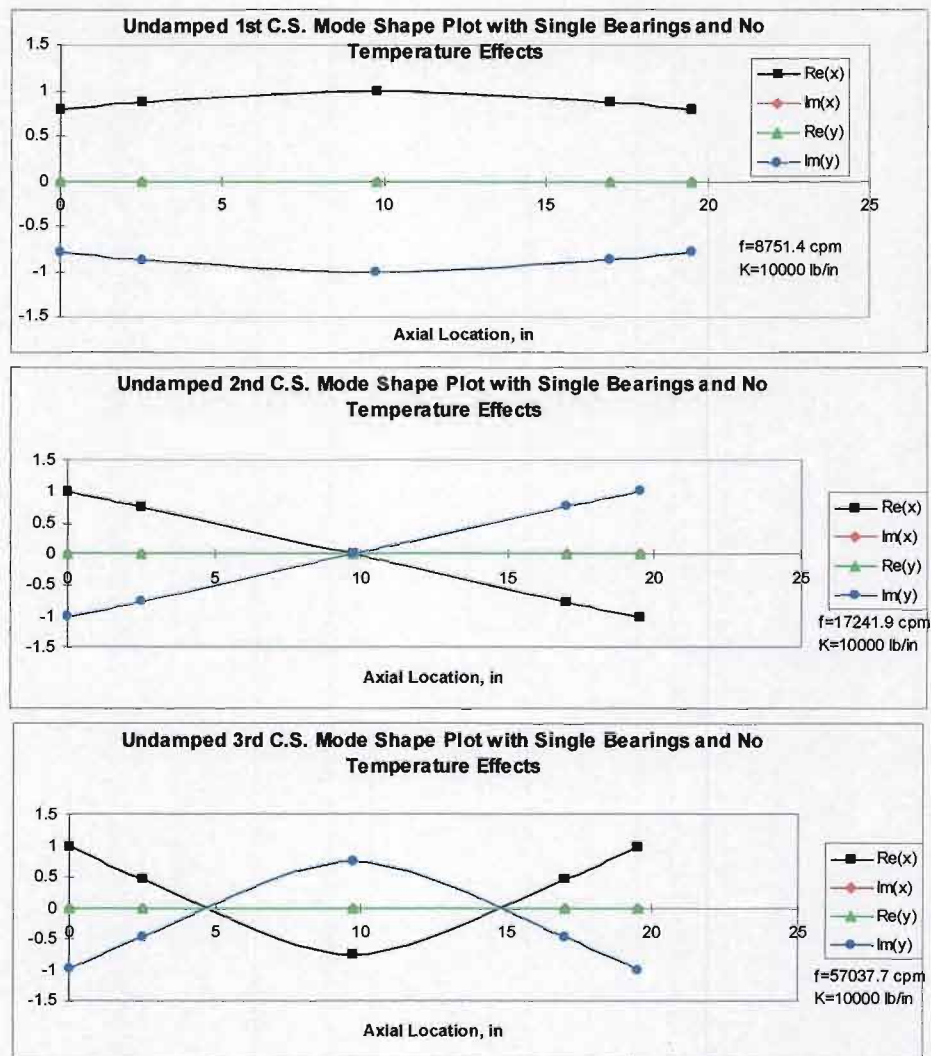


Figure 10: Undamped critical speed 1st, 2nd and 3rd mode shape plots using single support bearings.

4.3. Double Bearings

Using XLRotor double-bearing supports was modeled using the same geometry used in the single bearing model. This model is shown in Fig. 11.

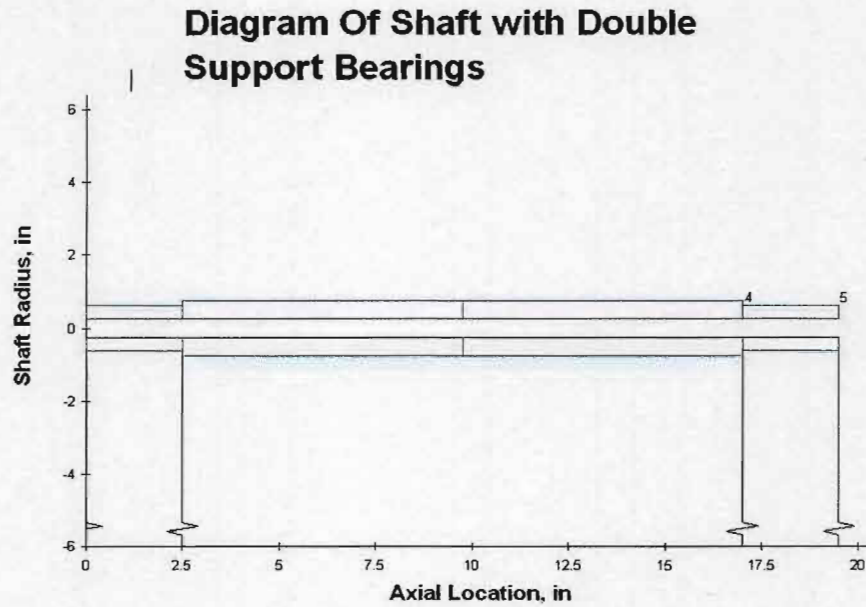


Figure 11: Double bearing supported shaft using XLRotor.

Using double bearings at the end of the heat pipe rotating rig the following undamped critical speed map is shown in Fig. 12.

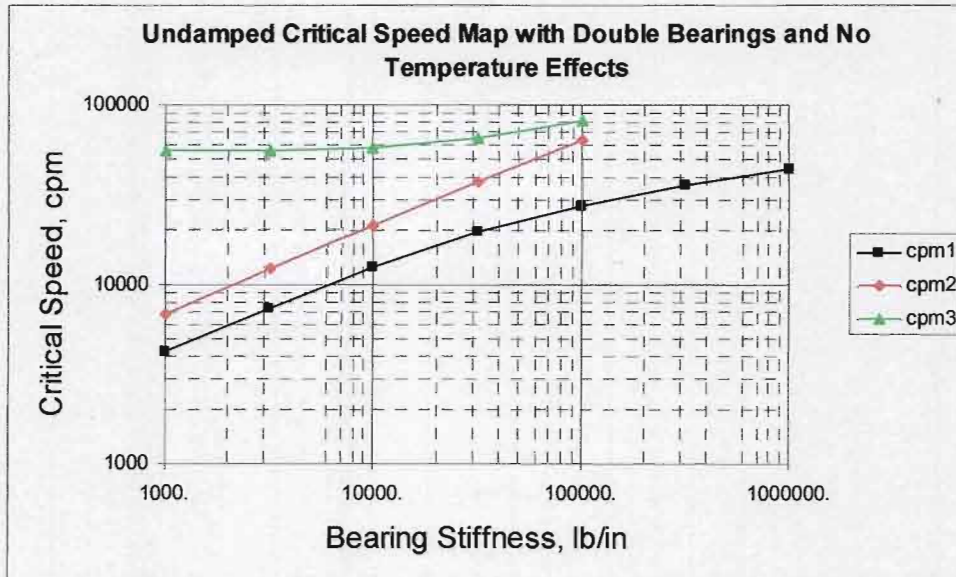


Figure 12: Undamped critical speed map for double support bearings.

XLRotor created the critical speed map (cpm) as a function of bearing stiffness using double bearings. A bearing stiffness of 10,000 lb/in is assumed for each bearing. Table 3 shows the critical speeds at different support stiffnesses using double bearings where the bold specifies the relevant critical speeds. The table does not contain critical speed values for the last two cpm's since these values exceed the 100,000 RPM limit set as a maximum boundary.

Table 3: Undamped critical speed table for double support bearings at different support stiffness values.

Stiffness	cpm1	cpm2	cpm3
1000.	4190.6	6898.5	54653.4
3162.	7339.4	12237.1	55387.2
10000.	12471.5	21598.6	57664.1
31623.	19664.4	37611.3	64353.9
100000.	27575.2	63649.3	80982.6
316228.	35756.5		
1000000.	44379.1		

Fig. 13 shows the mode shape plots using double support bearings located at the ends of the rotating rig. The first two mode shapes are the rigid body modes and the third is the bending mode of the double bearing system.

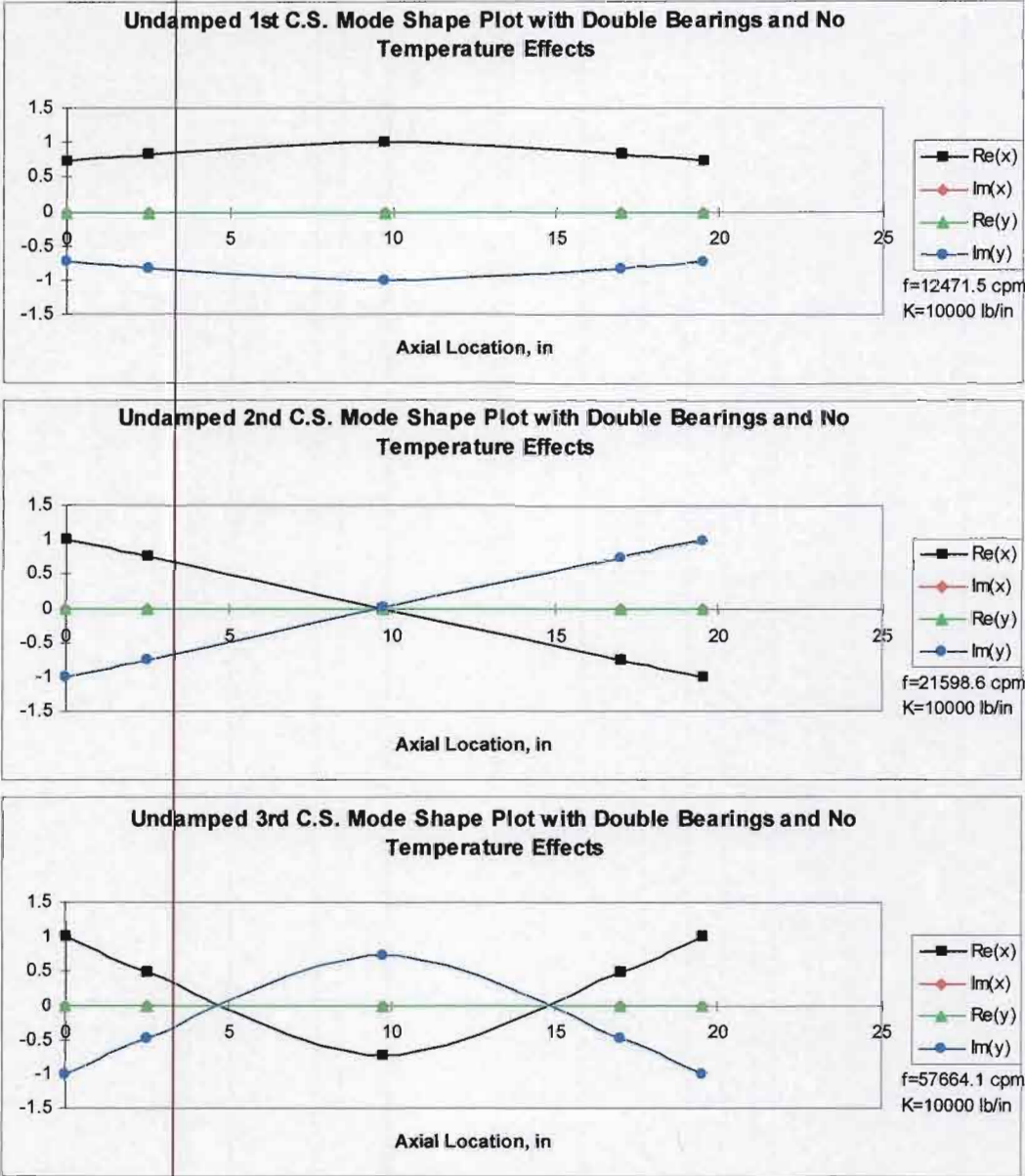


Figure 13: Undamped critical speed 1st, 2nd and 3rd mode shape plots using double support bearings.

4.4. Non-uniform Temperature Distribution

Using double bearings at the end of the heat pipe rotating rig and non-uniform temperature distribution the following undamped critical speed map and table were created. The non-uniform temperature distribution was achieved by assigning different modulus of elasticity at the points where a temperature increase was desired. Using XLRotor the system was modeled using double bearings and non-uniform temperature distribution included. This system is shown in Fig. 14.

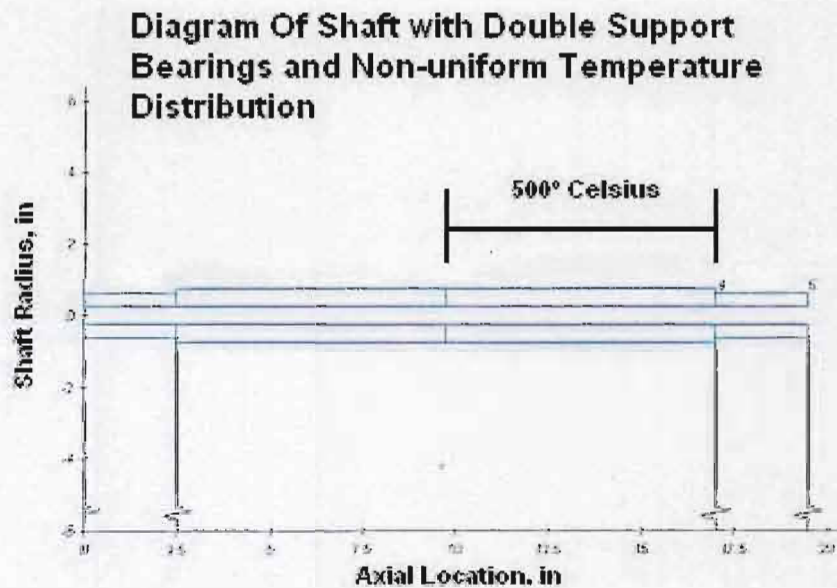


Figure 14: Double bearing supported and non-uniform temperature distribution shaft using XLRotor.

Using double bearings and non-uniform temperature distribution across a portion of the shaft the following undamped critical speed map was created, as shown in Fig. 15.

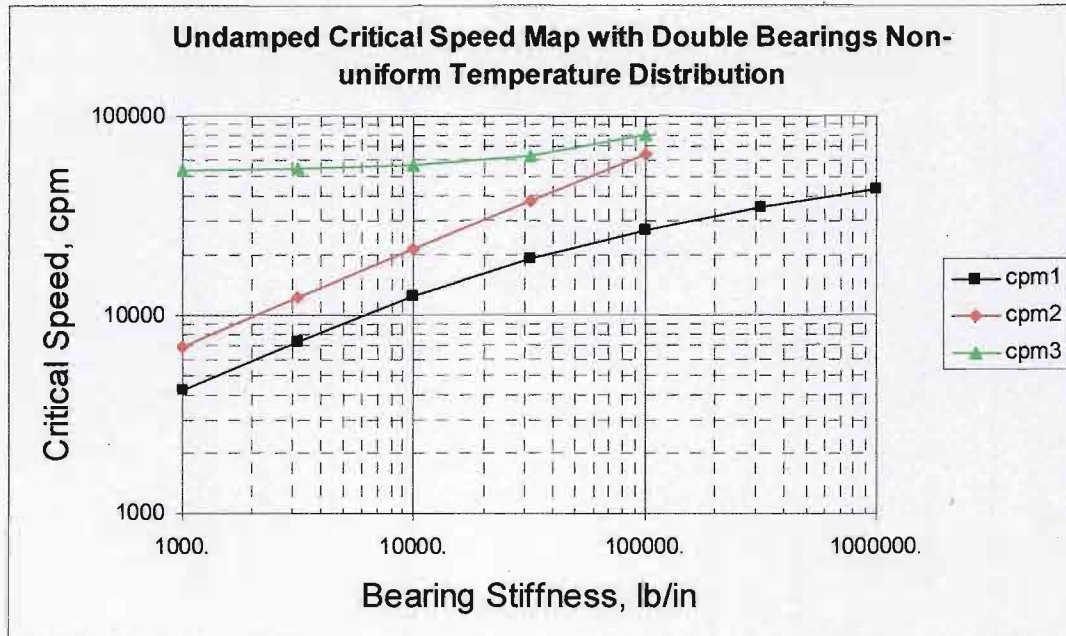


Figure 15: Undamped critical speed map for double support bearings and non-uniform temperature distribution.

Table 4 shows the critical speeds at different support stiffnesses using double bearings and a non-uniform temperature distribution where the bold specifies the relevant critical speeds. The table does not contain critical speed values for the last two cpm's since these values exceed the 100,000 RPM limit set as a maximum boundary.

Table 4: Undamped critical speed table for double support bearings and non-uniform temperature distribution at different support stiffness values.

Stiffness	cpm1	cpm2	cpm3
1000.	4188.4	6898.0	52861.4
3162.	7327.6	12234.5	53620.5
10000.	12414.1	21585.1	55972.6
31623.	19448.5	37551.0	62847.0
100000.	27086.6	63447.7	79727.8
316228.	35045.4		
1000000.	43432.1		

The following mode shape plots are using double support bearings located at the end of the rotating rig and a non-uniform temperature distribution. The first two mode shapes are the rigid body modes and the third is the bending mode of the double bearing system.

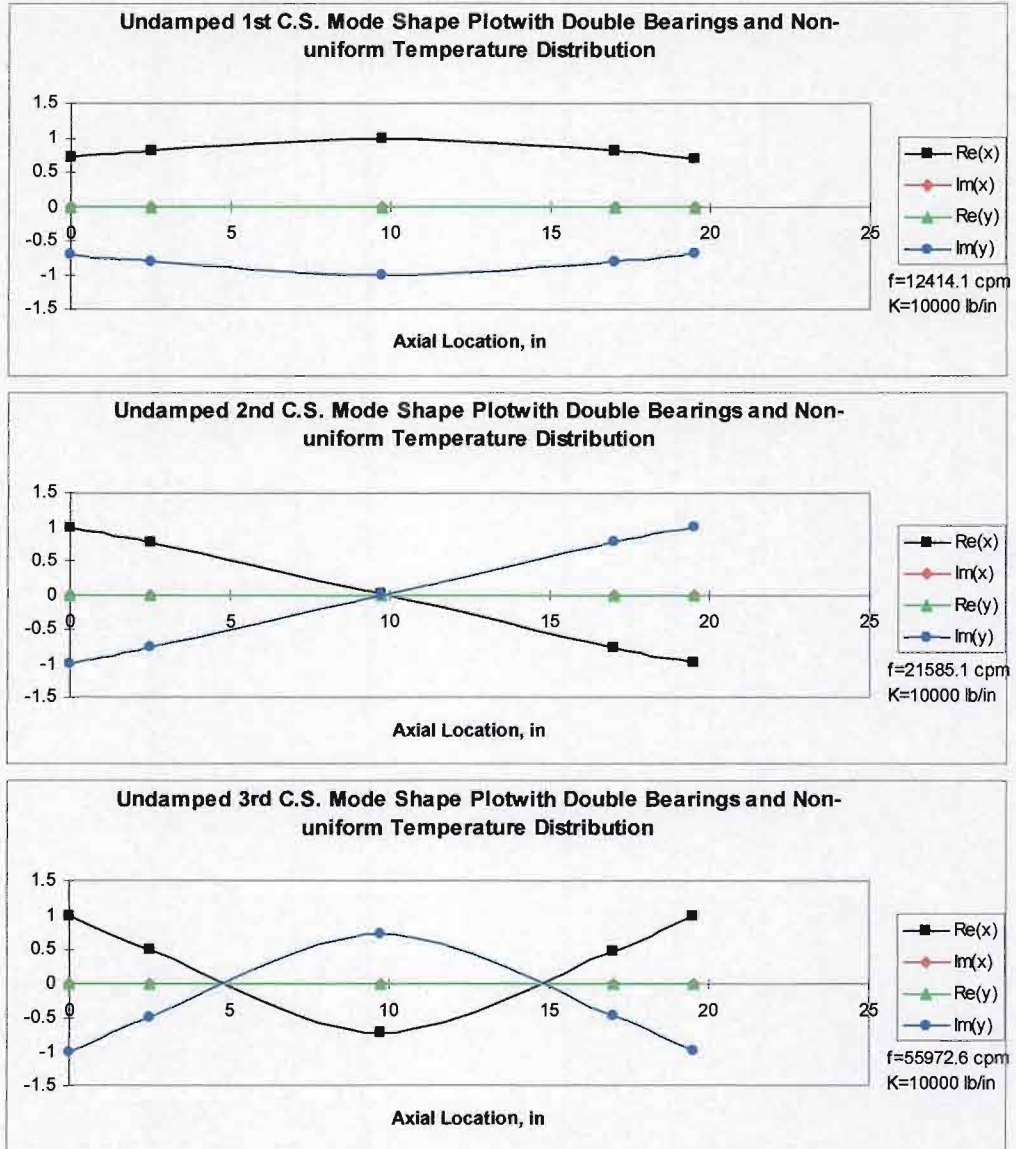


Figure 16: Undamped critical speed 1st, 2nd and 3rd mode shape plots using double support bearings and non-uniform temperature distribution.

4.5. Turbine Blades

Using double bearings at the end of the heat pipe rotating rig and modeling turbine blades as a weight at the middle of the testing specimen, the following XLRotor model was created, as shown in Fig. 17.

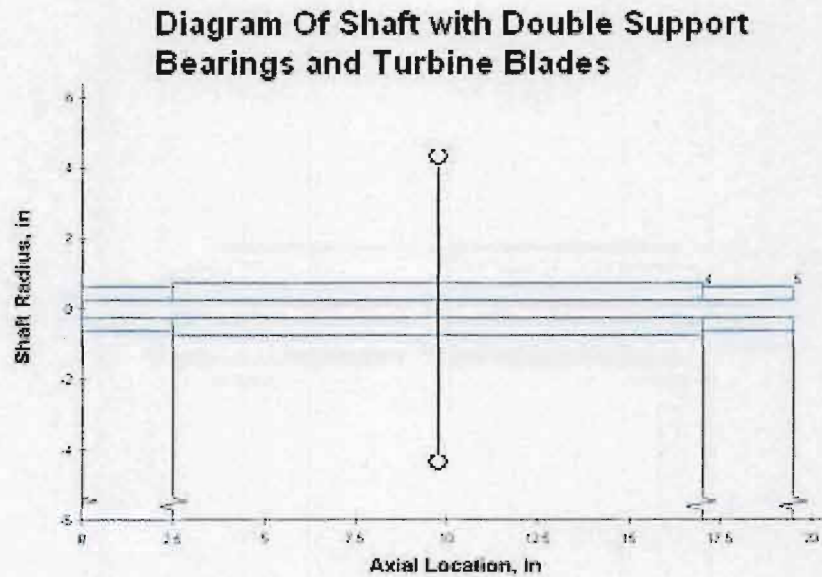


Figure 17: XLRotor model of a shaft using double support bearings and turbine blades simulated as a weight at the center.

XLRotor created the critical speed map (cpm) as a function of bearing stiffness using double bearings including turbine blades. A bearing stiffness of 10,000 lb/in is assumed for each bearing. Table 5 shows the critical speeds at different support stiffnesses using double bearings and turbine blades modeled as a weight at the center of the shaft. The bold specifies the relevant critical speeds of the research.

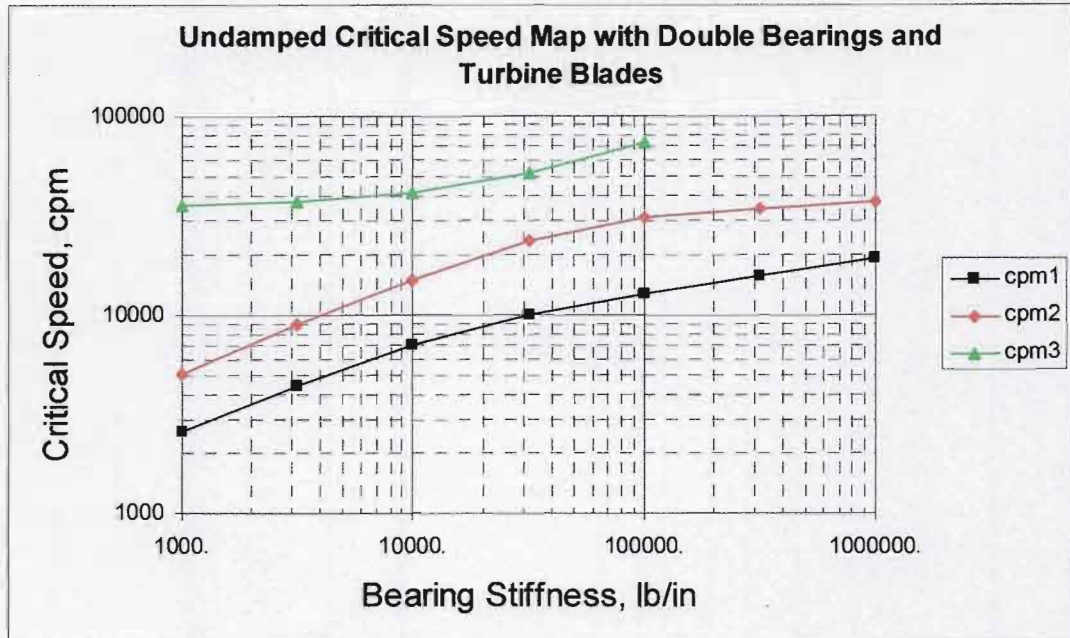


Figure 18: Undamped critical speed map for double support bearings and turbine blades.

Table 5: Undamped critical speed table for double support bearings and turbine blades at different support stiffness values.

Stiffness	cpm1	cpm2	cpm3
1000.	2580.1	5103.8	35819.1
3162.	4418.6	8950.1	37168.2
10000.	7084.9	15229.0	41152.5
31623.	10050.1	23695.5	51482.2
100000.	12723.3	30802.7	72831.4
316228.	15691.1	34617.0	
1000000.	19232.4	37080.8	

Fig. 19 shows the mode shape plots using double support bearings and turbine blades modeled as a weight in the center of the shaft. The first two mode shapes are the rigid body modes and the third is the bending mode of the double bearing system.

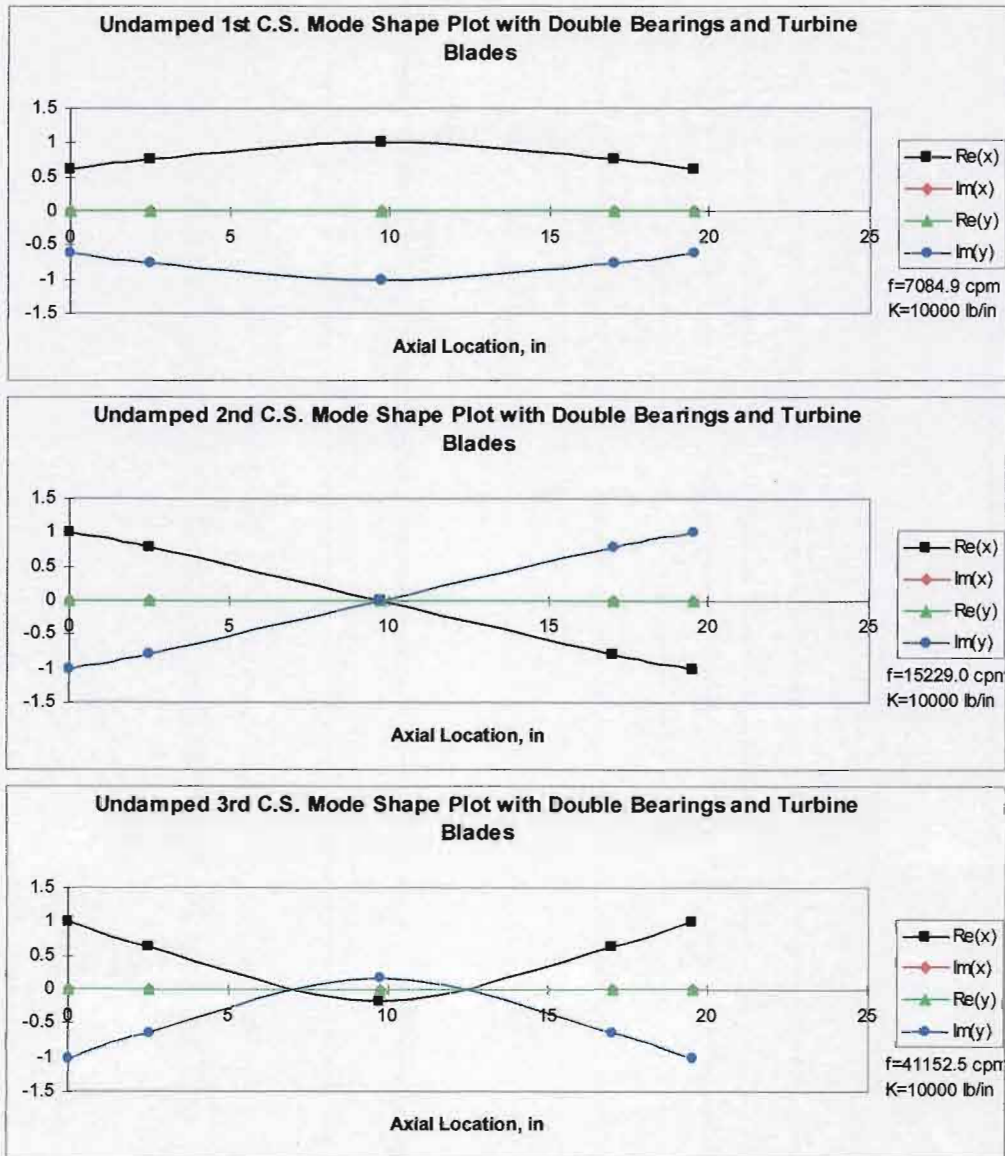


Figure 19: Undamped critical speed 1st, 2nd and 3rd mode shape plots using double support bearings and turbine blades.

5. Discussion and Conclusion

One of the main goals of this research was to test an ensemble of designs that would maximize the first critical speed of the rotating system. Using XLRotor single bearings were configured in order to establish if this design would meet the design requirements. It was found when using single support bearings the first critical speed of the system would be reached at 8,751 RPM's. The motor that will supply the rotating speed will reach an approximated speed of 10,000 RPM's. Since this is the target rotating speed, using single bearings would not meet the requirements. Using double support bearings was also analyzed using XLRotor. This configuration increases the support stiffness of the system. Using double bearings the first critical speed will be reached at 12,472 RPM's. This exceeds the benchmark of 10,000 RPM's that was desired. This configuration allows for valuable test data to be collected without worrying that the system might go into resonance. Another focus of this research was to explore the effects of a non-uniform temperature distribution. Since double bearings provide the adequate support, the effects of temperature will be explored using this configuration. In order to test for the temperature effect the modulus of elasticity was varied to simulate a non-uniform temperature distribution. The analysis shows that at 500 degrees Celsius a non-uniform temperature distribution will have a minimal effect on the critical speed of the system. Having non-uniform temperature distribution decreased the first critical speed of the system from 12,472 RPM's to 12, 414 RPM's. Using double bearings and having a non-uniform temperature distribution will be the first phase of the construction of the rotating rig. This configuration will be stable and will provide valuable test data without reaching any critical speeds.

6. Future Development

In order to construct a full scale rotating rig that test turbine components at service conditions, more extensive analysis far from the scope of this research will need to be performed. Using XLRotor proved to be a valuable tool in analyzing the rotor-dynamics of the system. However, the full version of the program will be needed to model the system more accurately and perform more complicated analysis. Since service conditions can reach rotating speeds in excess of 30,000 RPM's additional safety precautions will need to be considered. A testing chamber will need to be designed to withstand a catastrophic failure at these speeds. Failure in properly designing could cause injury to an operator. Also additional critical speeds will be reached at these conditions therefore; its effects on the system will need to be explored. Additionally, extensive fatigue and creep fatigue analysis of the system will need to be performed due to the higher temperatures and rotating speeds experienced.

7. Appendix: List of Symbols/Abbreviations

Nomenclature

- θ = tilt angle between the heat pipe centerline and the radial line of rotating axis, degree
 ρ = density, kg/m
 ω = angular velocity, rad/s
a,c = Constants
d = heat pipe diameter, m
 F_v = frictional coefficient of vapor flow
g = gravitational acceleration, m/s²
 h_c = average heat transfer coefficient in the condenser section, W/m²·K
 h_{fg} = latent heat of vaporization, J/Kg
 k_p = thermal conductivity of heat pipe wall, W/m·K
L = length of heat pipe, m
m = coefficient, 1/m
Q = heat transfer rate, W
r = heat pipe radius, m
T = temperature, K
W = flow rate of cooling air, kg/m³
Z = axial location of heat pipe, m
 Z_0 = revolving radius from the heat pipe bottom to the origin of the coordinate system, m

Subscripts

- a = adiabatic section
c = condenser
e = evaporator
eff = effective
i = inner
o = outer
s = surrounding
v = vapor phase
z = axial location

8. References

- [1] Ling, J., Cao, Y., Lopez, A., 2001, "Experimental Investigations of Radially Rotating Miniature High-Temperature Heat Pipes," *Journal of Heat Transfer*, Vol. 123, pp. 113-119.
- [2] Razani, A., Jankowski, T., Schmierer, E., Stewart, J., 2006, "Apparatus for Testing Rotating Heat Pipes," *AIAA/ASME Joint Thermophysics and Heat Transfer Conference*, AIAA 2006-3107.
- [3] Streby, M., Ponnappan, P., Leland, J., Bean, J., 1996, "Design and Testing of a High Speed Rotating Heat Pipe," *Institute of Electrical and Electronics Engineers*, 96301, pp. 1453-1458.
- [4] Ling, J., Cao, Y., 2000, "Closed-form analytical solutions for radially rotating miniature high-temperature heat pipes including non-condensable gas effects," *International Journal of Heat and Mass Transfer*, 43, pp. 3661-3671.
- [5] Song, F., Ewing, D., Ching, C. Y., "Experimental investigation on the heat transfer characteristics of axial rotating heat pipes," *International Journal of Heat and Mass Transfer*, Vol. 47, 2004, pp. 4721-4731.
- [6] Song, F., Ewing, D., Ching, C. Y., "Fluid flow and heat transfer model for high-speed rotating heat pipes," *International Journal of Heat and Mass Transfer*, Vol. 46, pp. 4393-4401.
- [7] Lee, J., Kim, C., 2001, "Heat transfer and internal flow characteristics of a coil-inserted rotating heat pipe," *International Journal of Heat and Mass Transfer*, Vol. 44, pp. 3543-3551.

- [8] Faghri, A., Gogineni, S., Thomas, S., 1992, "Numerical Analysis of Vapor Flow in an Axially Rotating Heat Pipe," American Society of Mechanical Engineers, Vol. 221, pp. 11-21.
- [9] Cao, Y., Chang, W., MacArthur, C., 1998, "An Analytical Study of Turbine Disks Incorporating Radially Rotating Heat Pipes," American Society of Mechanical Engineers, Vol. 361-3, pp. 103-111.
- [10] Salinas, D., Marto, P. J., 1991, "Analysis of an Internally Finned Rotating Heat Pipe," Numerical Heat Transfer, part A, Vol. 19, pp. 255-275.
- [11] Waowaew, N., Terdton, P., Maezawa, S., Kamonpet, P., Klongpanich, W., 2003, "Correlation to predict heat transfer characteristics of a radially rotating heat pipe at vertical position," Applied Thermal Engineering, Vol. 23, pp. 1019-1032.
- [12] Shtern, V., Zimin, V., Hussain, F., 2001, "Analysis of centrifugal convection in rotating heat pipes," American Institute of Physics, Vol. 13, pp. 2296-2308.